Nano Energy 80 (2021) 105555

Contents lists available at ScienceDirect

Nano Energy

journal homepage: http://www.elsevier.com/locate/nanoen

Full paper

Self-sustained autonomous wireless sensing based on a hybridized TENG and PEG vibration mechanism

Lu Wang [a,b,c,d,e,1], Tianyiyi He [c,d,e,1], Zixuan Zhang [c,d,e,1], Libo Zhao [a,b,*], Chengkuo Lee [c,d,e,**], Guoxi Luo [a,b], Qi Mao [a,b], Ping Yang [a,b], Qijing Lin [a,b], Xiang Li [b], Ryutaro Maeda [a,b], Zhuangde Jiang [a,b]

[a] *State Key Laboratory for Manufacturing Systems Engineering, International Joint Laboratory for Micro/Nano Manufacturing and Measurement Technologies, Xi'an Jiaotong University, Xi'an 710049, China*
[b] *School of Mechanical Engineering, Xi'an Jiaotong University, Xi'an 710049, China*
[c] *Department of Electrical & Computer Engineering, National University of Singapore, 4 Engineering Drive 3, 117576, Singapore*
[d] *Center for Intelligent Sensors and MfEMS, National University of Singapore, 4 Engineering Drive 3, 117576, Singapore*
[e] *National University of Singapore Suzhou Research Institute (NUSRI), Suzhou Industrial Park, Suzhou 215123, China*

ARTICLE INFO

Keywords:
Hybrid piezo/triboelectric nanogenerators
Broadband frequency
Tunable resonant frequency
TENG signal process
Self-powered accelerometer
Autonomous wireless sensing

ABSTRACT

Autonomous wireless sensor nodes (WSN) for information acquisition and status monitoring, play an important role in the boom area of the internet of things (IoT) and industry 4.0. Self-sustained power supply is an important pursuit in massive practical applications but yet to be developed. Here we propose a novel hybrid piezoelectric generator (PEG) and triboelectric nanogenerator (TENG) to form a novel self-sustainable WSN. The PEG consisting of a hinged-hinged PZT bimorph and two T shaped proof mass, has an output power of 6.5 mW excited in 25 Hz at 1.0 g. PEG also shows broadband characteristics thanks to the impact of the TENG and tunable frequency due to the axial force. 30 serial LEDs in sine vibration and 20 serial LEDs in shock vibration are lighted up with the proposed double voltage rectifier circuit by PEG, which can serve as alarming signals in vibration and drop monitoring. The triboelectric accelerometer shows good linearity with a sensitivity of 15 V/g in 0–1.5 g with an optimized gap of 1.5 mm. After low power design, Arduino nano and RF transceiver can be sustainably powered by PEG, and send the TENG acceleration signal wirelessly by Zigbee. A VR train monitoring demonstration has been conducted showing the great prospect of the self-sustainable WSN in harsh environments.

1. Introduction

Driven by rapidly developed internet of things (IoT) technology for harsh environment monitoring, self-sustained wireless sensor nodes (WSNs) are desired to remove the required labor-intensive task of changing the battery for WSNs in the remote area and harsh environment, where the battery lifespan is extended by energy harvesting technology [1–5]. Using the self-powered sensors based on the piezoelectric and/or triboelectric mechanisms have been investigated as promising solutions to reduce the power consumption of the whole WSNs [6–16]. More importantly, sizable energy collected from ambient and saved in the capacitor and/or battery is the ultimate approach to support the required power for the operation of wireless sensory data transmission of WSNs in the IoT framework [17–20].

There are many machines, robots, and devices used in remote area and harsh environments, such as drilling in mining, bridges, train rails, whose working status can be continuously monitored by embedded accelerometers, revealing the irregular vibration incidents where an abnormal acceleration value is detected. Status monitoring of various types of equipment[21], such as cars [22,23], train [24,25], pump [26], gearbox [27], and so on, especially relies on distributed WSNs using accelerometers. For example, the heavy haul railway has nearly 100 carriages and wheelsets. The wheelset bears continuous vibration in the range of < 2 g, 10–40 Hz during its operation [28,29]. Accelerometers

* Corresponding author at: State Key Laboratory for Manufacturing Systems Engineering, International Joint Laboratory for Micro/Nano Manufacturing and Measurement Technologies, Xi'an Jiaotong University, Xi'an 710049, China.
** Corresponding author at: Department of Electrical & Computer Engineering, National University of Singapore, 4 Engineering Drive 3, 117576, Singapore.
E-mail address: elelc@nus.edu.sg (C. Lee).
[1] These authors contributed equally.

https://doi.org/10.1016/j.nanoen.2020.105555
Received 4 August 2020; Received in revised form 30 September 2020; Accepted 26 October 2020
Available online 29 October 2020

can continuously monitor axle box vibration, and regularly report the acceleration levels as a WSN to the senor hub, e.g., the head of the train. When the abnormal sensor data is measured, which indicates the axial or bears need to overhaul or even in the broken situation, the alarm signal will be notified to the central control office at the station.

So far, the self-powered accelerometers have been reported by a few groups with various designs and mechanisms for different applications including healthcare, IoT, and harsh environment monitoring [30–35]. For instance, Liu et al. provided theoretical study and developed a self-powered accelerometers with high sensitivity [36]. Shi et al. developed a self-powered gyroscope ball with a ball-shape design where the hollow sphere contains several steel balls inside to move freely on the inner surface for triboelectric output generation [33]. To achieve a broadband behavior, Gupta reported a hybrid energy harvester with a non-linear stiffing effect introduced by mechanical stoppers, where the TENG device is located for acceleration sensing [35]. For another instance, a self-powered multifunction motion sensor with a magnetic-regulated TENG is reported, where the TENG consists of a free-standing magnetic disk on a PTFE plate, but with a limitation of in-plane accelerations and motion status detection [32]. A low-frequency ($<$ 12 Hz) spring-mass system integrated with TENG is developed as a vibration accelerometer for railway state monitoring, but the minimal detected acceleration level is higher than 1 m/s^2 possibly due to the large gap between the triboelectrification layers in the structure [30]. Besides, the adjustable resonant frequency has rarely achieved with the reported designs. Complex signal acquisition circuits for signal processing of the TENG accelerometer could be power consuming, especially considering the power required for wireless transmission.

Energy harvesting technology then has emerged a promising solution to provide renewable and sustainable energy to power the WSNs. Despite renewable energy such as solar and wind has been developed and deployed outdoors successfully [37,38]. It is hard to get renewable energy from the dark and narrow space inside of most types of equipment, such as axial box and gear box. Luckily, there is wealthy vibration energy existing in various equipment during operation especially in low frequency band. Vibration energy harvesting can play an important role to supply electrical power for WSNs by piezoelectric [39], electrostatic [40], electromagnetic [41], and triboelectric [42] or their hybrid approaches [43–45]. Among them, piezoelectric and triboelectric approaches are reported with higher power density [46]. For example, a honeycomb structure inspired triboelectric nanogenerator is reported with a high power density of 50 W/m^3 (25 Hz, 2.0 mm vibration amplitude) [47] and a high output power of 227 mW has been achieved with a piezoelectric nanogenerator of small device size (Φ48 mm $\times$ 27 mm) [48]. The design of mechanical energy conversion systems generally focuses on the frequency match with the ambient vibration to maximize the harvested energy at the resonant state.

The piezoelectric generators (PEG) mainly deploying a lead zirconate titanate (PZT) based monomorph and/or bimorph cantilever or beam in the centimeter-size range, where such fundamental mechanical transducers can convert transverse vibration into the longitudinal strain, and AC output is generated when the PZT cantilevers/beams are under vibration [17–20]. Usually, a proof mass is added to increase the mechanical energy and decrease the resonant frequency [49,50]. The stopper design is a practical method to achieve broadband characteristics and overload protection [51,52]. To increase the overall output power of the PEG, frequency-up-conversion mechanisms have been investigated and reported as well [53,54]. Besides, to compensate for the mismatch between device resonant frequency and excitation frequency, applying the axial force to the bulked beam has been proven to be an effective approach of frequency tuning. Adjust the axial force is an indirect and convenient approach to adjust the stiffness of the system due to it keep away from the moving part. Fixed or hinged beam can tuning the frequency by adjusting the screw rotation of the bolt [55]. Cantilevered piezoelectric beam with magnet tip mass can obtained different natural frequencies by adjusting the gap between the magnets [56]. The combination of these technologies will bring more flexibility and adaptability to low-frequency and broadband vibration energy harvesting, leading to desirable performances for various applications [57–61].

Vibration-based triboelectric nanogenerator (TENG) aiming at low-frequency vibration energy harvesting has been studied [62–64]. For example, Bhatia et al. has reported a tandem TENG for scavenging mechanical vibrational energy with vertical contact-separation mode [65]. Shi et al. reported a triboelectric buoy ball harvesting vibrational energy from ocean waves working on the sliding mode [66] A hybridized TENG and PEG vibration mechanism will combine advantages of high voltage in TENG and high current output in PEG. Most previous works of the hybrid generators are only used for harvesting energy to enhance the output power [48,60,67–72] or for multifunctional sensing [31,73–75]. However, direct parallel or series connection of the TENG and PEH would cause the mismatching of the impedance between them. In this regard, it is more reasonable to separately utilize the outputs of the TENG and PEG in the vibration system.

Self-sustained WSNs are very crucial for IoT applications in remote areas and harsh environments. The sustainable power supply required for the microcontroller unit (MCU) and radio frequency (RF) transceiver is typically at a few milliwatt level of power consumptions. It still remains a great challenge for the realization of the self-sustained autonomous WSN. Wen Feng et al. proposed a novel approach to realize the direct wireless transmission of the triboelectric sensory information requiring no external power, by simply combining a TENG textile, a mechanical switch, and a coil to form an RLC circuit [76]. Secondly, with the aid of the low power consumption BLE module, He et al. demonstrated a self-sustainable healthcare monitoring system for temperature and humidity sensing, powered by scavenged energy from foot motions through TENG textiles [77]. Although some commercial WSNs have very low power consumption at the microwatt level, such as Bluetooth temperature and humidity sensors, which are commonly used for TENG or PEG energy harvesting applications [18,78], there is still a mismatch between the output power of nanogenerators and device power consumption. Therefore, in most cases, it requires a long time for the PEG or TENG to charge up a capacitor with energy high enough to power the WSNs, due to the large gap between the output power and operation power. As such, the operation of the self-sustained WSNs is yet to be really sustainable for most of the hardware solutions. To address this issue, duty cycle design should be implemented to make WSN have shorter operation time and longer rest time to reduce average power consumption, which may realize the programmable and reconfigurable WSNs.

In this paper, we present a novel hybrid generator and propose a self-sustained WSN based on a hybridized TENG and PEG vibration mechanism. The hybrid nanogenerator is thoroughly investigated by simulation and experiments to achieve broadband behavior and tunable resonant frequencies. The TENG functioning as the self-powered acceleration sensor is also optimized to achieve a good sensing performance. The Arduino-based programmable accelerometer WSN is designed in a low power consumption style. In the self-sustainable WSN, the TENG output as the acceleration sensing signal is fed into the MCU, while the PEG sustainably supplies power to the MCU and RF transceiver to transmit the acceleration signal out wirelessly in diversified IoT applications as shown in Fig. 1(a).

2. Structure and working mechanism

The structure design of the proposed hybrid generator is shown in Fig. 1(b), in which the device consists of one PEG and two TENGs. A PZT bimorph is hinged-hinged mounted. Two T shaped copper proof masses are bonded with the PZT bimorph by foam, which can reduce concentrated stress. The cube package material is polymethyl methacrylate (PMMA). The bolt and nut mounted at one side of the cube package can give an axial force to tune the resonant frequency of PZT bimorph. Two

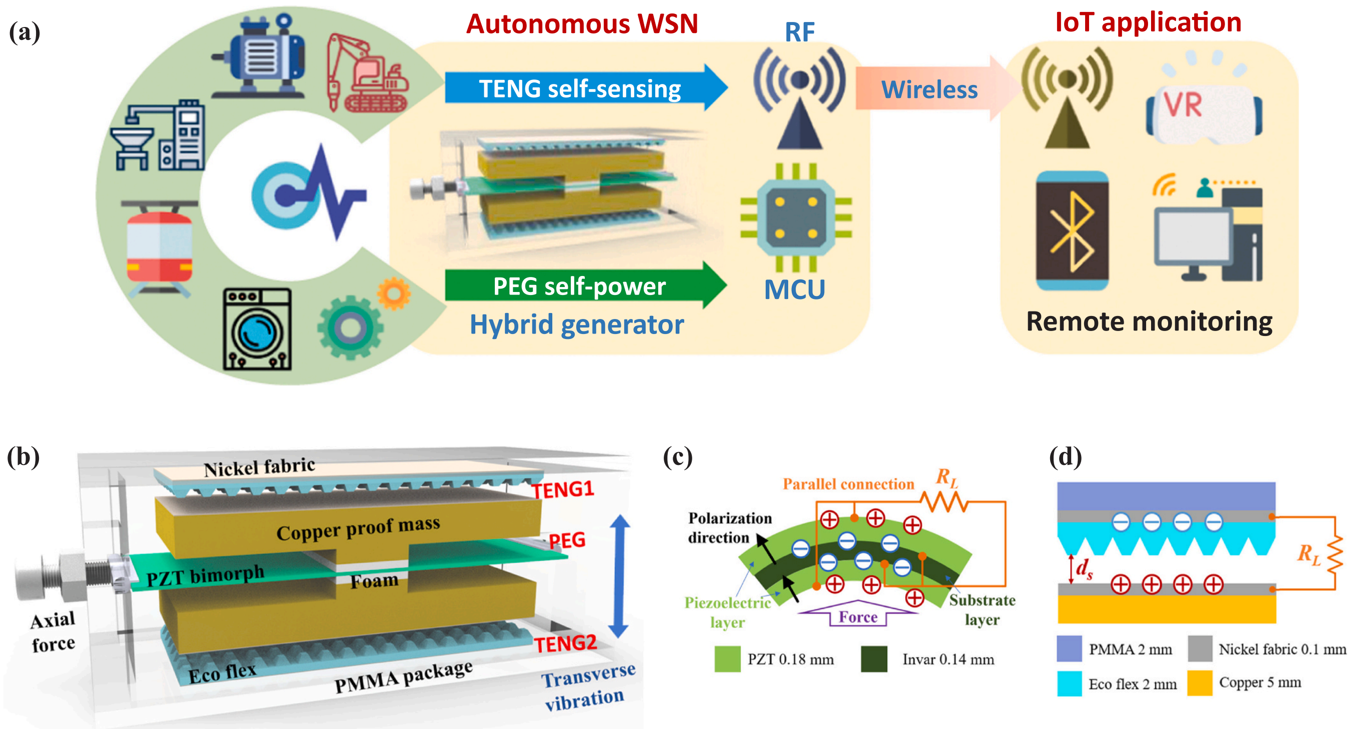

Fig. 1. (a) Schematic illustration of autonomous WSN for equipment vibration monitoring. (b) Structure design of hybrid TENG and PEG module. (c) Working principle of PEG. (d) Working principle of TENG.

TENGs function as the stoppers for PEG overload protection and generate signals in contact-separation mode. Fig. 1(c) shows the deformation of the PZT bimorph as the working principle of PEG. Excited by ambient vibration, the transverse inertial force of proof mass will induce longitudinal strain in PZT bimorph. Due to the d31 piezoelectric effect, an alternating current will be generated in a parallel connection of two piezoelectric layers, and the polarization direction of the piezoelectric layers is from bottom to top. Fig. 1(d) shows the "contact-separation" working principle of TENG. A nickel fabric as a positive electrode is bonded with copper proof mass for a moving part. Eco flex with pyramidal synaptic array structure is selected as the negative triboelectric material for its soft stiffness and sufficient contact to generate more triboelectric charges. The flat side of eco flex is bonded with PMMA by another nickel fabric as a negative electrode for the substrates.

The schematic diagram of the working cycles of the hybrid generator is shown in Fig. S1. When contact occurs, the negative triboelectric charges are transferred from the nickel fabric on the proof mass to eco flex. In the sine excited state, PEG will vibrate and PZT will generate sine voltage signal accordingly. The separation between TENG will also generate a sine voltage signal due to electrostatic induction. The two TENGs located above and below the proof mass operate in the opposite phases.

To further elucidate the contribution and the creative engineering design of this work clearly compared to the current self-sustainable wireless IoT systems, we have summarized some recent works in Table 1 as shown below. For most of the reported works, the systems consist of the developed energy harvesters and commercial sensors (e.g., temperature sensor, humidity sensor, accelerometer) in two separate sections. For example, He et al. developed a triboelectric-piezoelectric-electromagnetic hybrid nanogenerator as the power source of a self-powered wireless monitoring system, which detects the acceleration and temperature of the hybrid nanogenerator by the integrated commercial sensors on the circuit board [48]. Similarly, Jin et al. proposed a self-powered wireless sensor based on a vibrational hybrid nanogenerator and a commercial temperature/humidity sensor board for the train monitoring system [24]. However, the vibrational status of the nanogenerator, which is considered as an essential characteristic to reveal the proper functionality of the train, isn't taken into account in their system. Recently, Khan et al. developed a wireless sensing system realized with an all-in-one TENG, i.e., the device consists of multiple TENGs with one of them serving as an oscillation frequency sensor and the others functioning as power sources [79]. Though the wireless sensing system has a high integrity, the sensing function is limited to the vibrational frequency and with poor linearity from 10 Hz to 60 Hz. In our self-sustainable WSN, we integrate the PEG and TENG in a single device with the PEG harvesting energy from the external vibration and the TENG monitoring the acceleration of the external stimuli, without the need to introduce commercial sensors to the whole system. Besides, good linearity has been achieved with the TENG sensor in a sensing range up to 1.5 g through the structure optimization. Moreover, the adjustable stopper distance and the axial force endows the device a good adaptability to different ambient environment aiming at diversified applications as illustrated in Fig. 1.

Moreover, compared with the silicon-based capacitive accelerometer, the triboelectric accelerometer does not need an additional power supply. The self-power piezoelectric accelerometer has low sensitivity in low-frequency detection and requires the charge amplifier. The sensitivity of the self-generating signal of the triboelectric accelerometer is very high even under low-frequency excitation, which can reach tens of volts or even up to 100 volts. Moreover, the triboelectric accelerometer is advantageous in terms of low cost, easy assembly, and the simple subsequent signal processing circuit. The limitation of the triboelectric accelerometer is that the resolution is low and the vibration waveform has poor tracking performance at current states. In this case, the triboelectric accelerometer is more suitable for vibrational amplitude monitoring or shock counting.

3. Design and performance of PEG harvester

PEG is firstly designed by finite element analysis (FEA) in COMSOL.

Table 1
Review of recent self-sustainable wireless IoT.

Ref.	Device features	Power source	Sensing mechanism	Application	Volume	Charging
[20]	Triboelectric-electromagnetic hybrid nanogenerator (powering)	Peak power: TENG (0.36 mW) EMG (18.6 mW) at wind speed of 9 m/s	Commercial temperature and humidity sensor	Self-powered wind speed sensing	$10 \times 8 \times 6$ cm^3 (estimated)	1 mF 20 V 30 s
[48]	Triboelectric-piezoelectric-electromagnetic nanogenerator (powering)	Peak power: TENG (78.4 μW) EMG (36 mW and 38.4 mW) PEG (122 mW and 105 mW) at 20 Hz	Commercial temperature sensor and triaxial accelerometer	Vibration and temperature monitoring	$\Phi 4.8 \times 2.7$ cm^3	1 mF 8 V 250 s
[24]	Triboelectric-electromagnetic nanogenerator (powering)	Peak power: TENG (0.34 mW/g) EMG (0.12 mW/g)	Commercial temperature and humidity sensor	Self-powered temperature and humidity sensing	$\Phi 4 \times 3$ cm^3 (estimated)	4.7 mF 3 V 22 s
[79]	Triboelectric nanogenerators (powering and sensing)	Peak power: TENG (10 mW)	TENG vibration sensor	Self-powered vibrational frequency sensing	$6.5 \times 6.5 \times 2$ cm^3	1 mF 3 V 110 s
[80]	Rotating triboelectric nanogenerator (powering and sensing)	RMS power: TENG (44.4 μW) at 300 rpm	TENG speed sensor	Self-powered wind speed sensing	$\Phi 10 \times 1.6$ cm^3	0.1 mF 5 V 15 s
[81]	Triboelectric-electromagnetic nanogenerator (powering)	Peak power: TENG (15.21 μW) EMG (1.23 mW)	Commercial temperature sensor	Self-powered temperature sensing	$16.7 \times 10 \times 4$ cm^3	0.1 mF 3 V 200 s
This work	Piezoelectric (powering) and triboelectric (sensing) nanogenerator	RMS power: TENG (3.07 μW) PEG (6.5 mW) at 25 Hz 1.0 g	TENG acceleration sensor	Self-powered acceleration sensing	$7 \times 3 \times 2.9$ cm^3	1 mF 20 V 25 s

The modal analysis will show the first eigenfrequency of the PEG. The mass of the vibration system has a great effect on eigenfrequency. The T shaped proof mass consists of a small cube mass with length of 10 mm and a big cube mass with length of 50 mm. The separation of 3 mm between big cube mass and PZT is equal to the sum of the thickness of the small cube mass and the thickness of the foam, which ensures the moving space of the PZT bimorph. Since the mass largely affects the system eigenfrequency, the big cube mass thickness can be changed to tune the system eigenfrequency in the design phase. Fig. 2(a) shows the curves of first eigenfrequency change with different big mass thickness. Indeed, increasing the big cube mass thickness will decrease the first eigenfrequency. An appropriate mass thickness can be chosen to match the resonant frequency with the vibration of equipment where the PEG is mounted. In this research, the big cube mass thickness is set to 5 mm to match 25 Hz equipment vibration.

Stress check is our main concern in the frequency response analysis. Displacement and the stress nephogram in 25 Hz at 0.5 g are obtained by the dynamic analysis as shown in Fig. 2(d), and the part of PZT surface stress and deflection are shown in Fig. 2(e, f). The bonding edge of foam and PZT layer has the maximum PZT stress. Soft foam bonding can avoid stress concentration at the bonding edge. The center of the beam has the maximum deflection.

The curves of maximum PZT stress and open-circuit (load resistance of 1 MΩ) voltage with different accelerations in 25 Hz as shown in Fig. 2(b). Both of them increase linearly when the acceleration level increases. Although the higher the stress, the higher the output voltage, the maximum stress should be limited to the allowable stress to avoid material cracking. The allowable stress of the PZT ceramics is 80 MPa. Ceramic cracks will occur and the power generation performance will be reduced if the maximum PZT stress exceeds the allowable stress.

As shown in Fig. 2(c), the maximum PZT stress increases linearly with the vibration displacement of proof mass. To avoid the excessive stress applied to the PZT, the TENG can be set on top and bottom of the proof mass as a stopper to limit the vibration displacement within 2.2 mm, which is the boundary displacement for allowable stress. The distance between proof mass and eco flex is considered as the stopper distance. This research selects 3 different kinds of stopper distance, 1.0 mm, 1.5 mm, 2.0 mm, respectively in prototype performance experiments.

Fig. 2(g) shows the experiment results of frequency response voltage (load resistance of 1 MΩ) curves of PEG with different stopper distance ds = 1.0, 1.5, 2.0 mm. The resonant frequency is near 25 Hz and the phenomenon of clipping peak appears near the resonant frequency. The stiffness becomes sharply harder when PEGs impact with TENG (Fig. S2), and the nonlinear extension of frequency band occurs. Broadband behavior is achieved thanks to the TENG as the stopper. PEG with ds = 1.0 mm has a wider broadband range but lower voltage output. PEG with ds = 2.0 mm has a narrower broadband range but higher voltage output. The bigger the acceleration level, the wider broadband range. For PEG with ds = 1.0 mm, the band for normal operation of TENG in 1.0 g acceleration is 21–28 Hz and 20–30 Hz in 1.5 g acceleration.

Despite big cube mass thickness can be changed to tune the system eigenfrequency in the design phase, there will be some mismatch between the actual excitation frequency and the resonant frequency of PEG prototype. Therefore, an axial force is applied to tune the resonant frequency of PEG. A theoretical model and analysis is provided in Note S1. Eq. (1) indicates the relation between axial force P and the open-circuit resonant frequency f_r of PEG. As shown in Fig. 2(h), screw nut connection is applied at one side of the hinged supporter. The axial stress can be estimated by screw rotation (Note S2). Eq. (2) indicates the relation between screw rotation angle θ and the axial force P. PEG resonant frequency tuning under different axial forces is shown in Fig. 2(h). It can be observed that the PEG resonant frequency decreases from 25 Hz to 19 Hz along with the axial force varies from 0 N to 12 N.

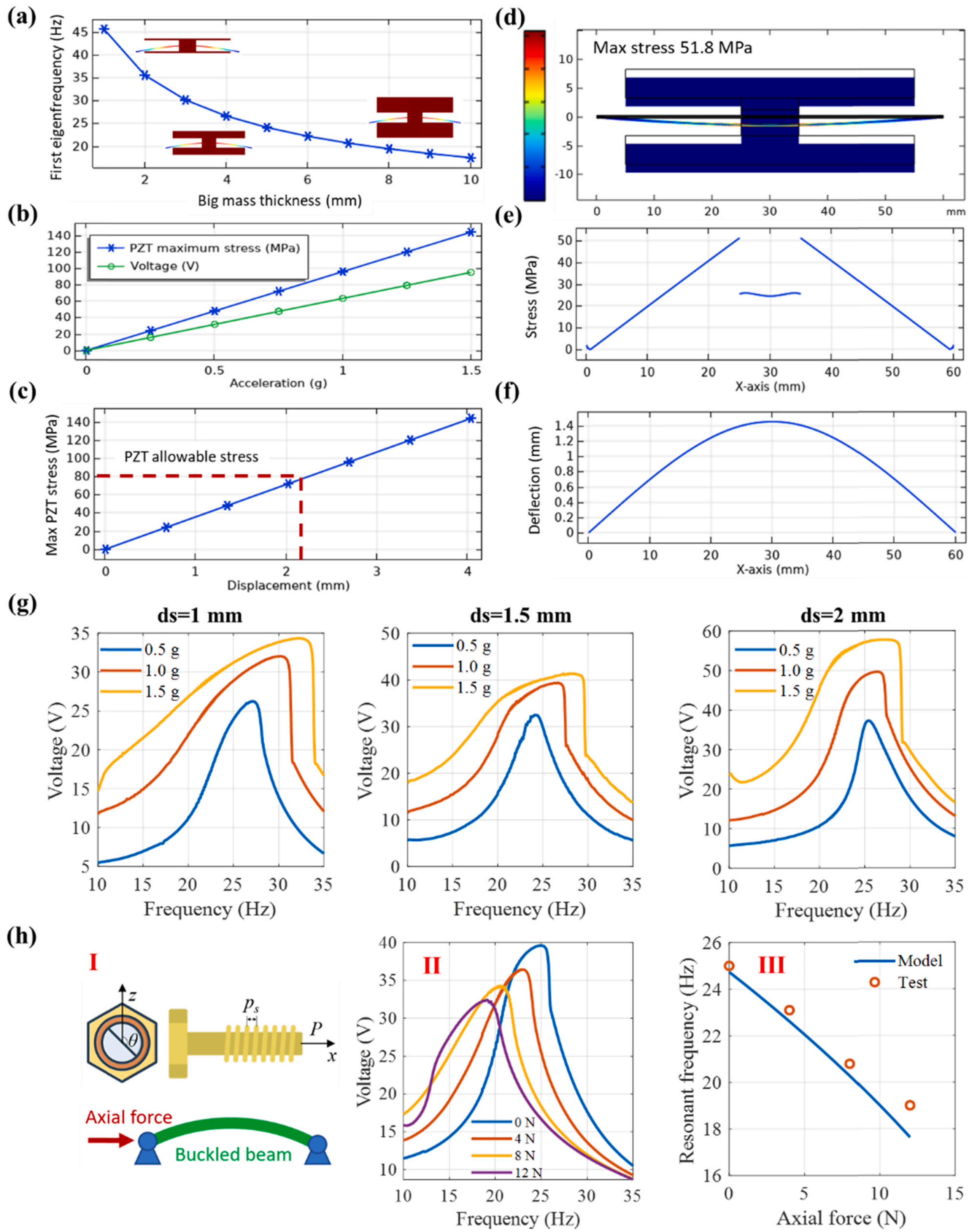

Fig. 2. Design and analysis of PEG in COMSOL (a) First eigenfrequency with different big mass thickness. (b) PZT maximum stress and voltage under different acceleration. (c) PZT maximum stress with different displacement. Vibration analysis in 0.5 g acceleration at 25 Hz: (d) first resonant modal, (e) stress on the surface of PZT and (f) deflection along the beam in resonant state. Broadband vibration when TENG impacted: (g) experimental frequency response voltage curves of PEG with different ds = 1.0, 1.5, 2.0 mm under acceleration of 0.5, 1.0, 1.5 g. (h) PEG resonant frequency tuning under different axial force: (I) Schematic diagram; (II) Experimental frequency response voltage curves of PEG with ds = 1.5 mm under acceleration of 1.0 g; (III) Comparison of theoretical and experimental results.

$$f_r = 2\pi\sqrt{\left(1-\frac{P}{P_{cr}}\right)\frac{\pi^4 EI}{2L^3}\Big/\left(M+\frac{m}{2}\right)\left(1-k_e^2\right)} \tag{1}$$

Where P_{cr} is the Euler critical buckling load, EI is the bending rigidity of the beam, L is the beam length, m is the beam mass, M is the proof mass, and k_e is the electromechanical coupling coefficient.

$$P = \frac{EAp_s\theta}{2\pi L} \tag{2}$$

Where EA is the compressive stiffness of the beam, p_s is the screw distance.

4. Design and performance of the TENG acceleration sensor

According to the acceleration sensing mechanism of TENG, the stopper distance *ds* affects the range and linearity of the triboelectric accelerometer, which should be discussed and investigated. The stopper distance in the prototype can be controlled by the height of the two hinged supporters. In the vibration experiment at a fixed frequency of 25 Hz, hybrid generators with three kinds of stopper distance are tested in 6 acceleration levels, i.e., 0.25 g, 0.5 g, 0.75 g, 1.0 g, 1.25 g, and 1.5 g, respectively, where the 1.0 g equals to 9.8 m/s^2. Their time response voltage curves are shown in Fig. 3(a). The amplitudes of two TENG signals both increase as the acceleration level arises. The amplitude of PEG signal increases with the acceleration first but quickly saturates to the maximum value due to the limitation of the TENG stopper distance. For the stopper distance of 1 mm, the PEG signal keeps stable as acceleration level arises beyond 0.5 g, with TENG output of 18 V and PEG output of 32 V at 1.5 g. For the stopper distance of 1.5 mm, the PEG signal keeps stable as acceleration level arises beyond 0.75 g, with TENG output of 23 V and PEG output of 42 V at 1.5 g. For stopper distance of 2 mm, the PEG signal keeps stable as acceleration level arises beyond 1.0 g, leading to TENG output of 30 V and PEG output of 47 V at 1.5 g. It is noted that a small stopper distance will limit the output of TENG and PEG, but a large stopper distance will cause no impact to the TENG at low acceleration levels and may cause the overload of the PEG. Therefore, the hybrid generator with the stopper distance of 1.5 mm is an optimal choice considering the large outputs from both TENG and PEG and the prevention of overload of the PEG.

To calibrate TENG as an accelerometer, Fig. 3(b) shows the rectified filter signal process of TENG. Here, TENG stopper distance of 1.5 mm excited in the acceleration of 1.0 g. TENG1 and TENG2 have similar sinusoidal signals with the same frequency but different phases. Therefore, they should be rectified by a rectifier (DF-10) separately before parallel connection. To get a stable direct current (DC) signal, a filter capacitor C_F of 1.3 nF is used. Fig. 3(c) shows the rectified filter TENG voltage at different accelerations in 5 min. They have very narrow drift without overlapping and can be identified easily with a high sensitivity of 15 V/g in 0–1.5 g. For accelerometer reading circuit, the voltage range of analog port in Arduino is within ± 5 V. Therefore, the load resistance of 6 MΩ is applied to limited TENG voltage to that range. Finally, voltage values of each TENG with different stopper distance at 6 acceleration levels are drawn in Fig. 3(d). It can be observed that TENG voltage signal with a stopper distance of 1.5 mm has the optimal linearity with the acceleration levels. Therefore, the 1.5 mm distance is

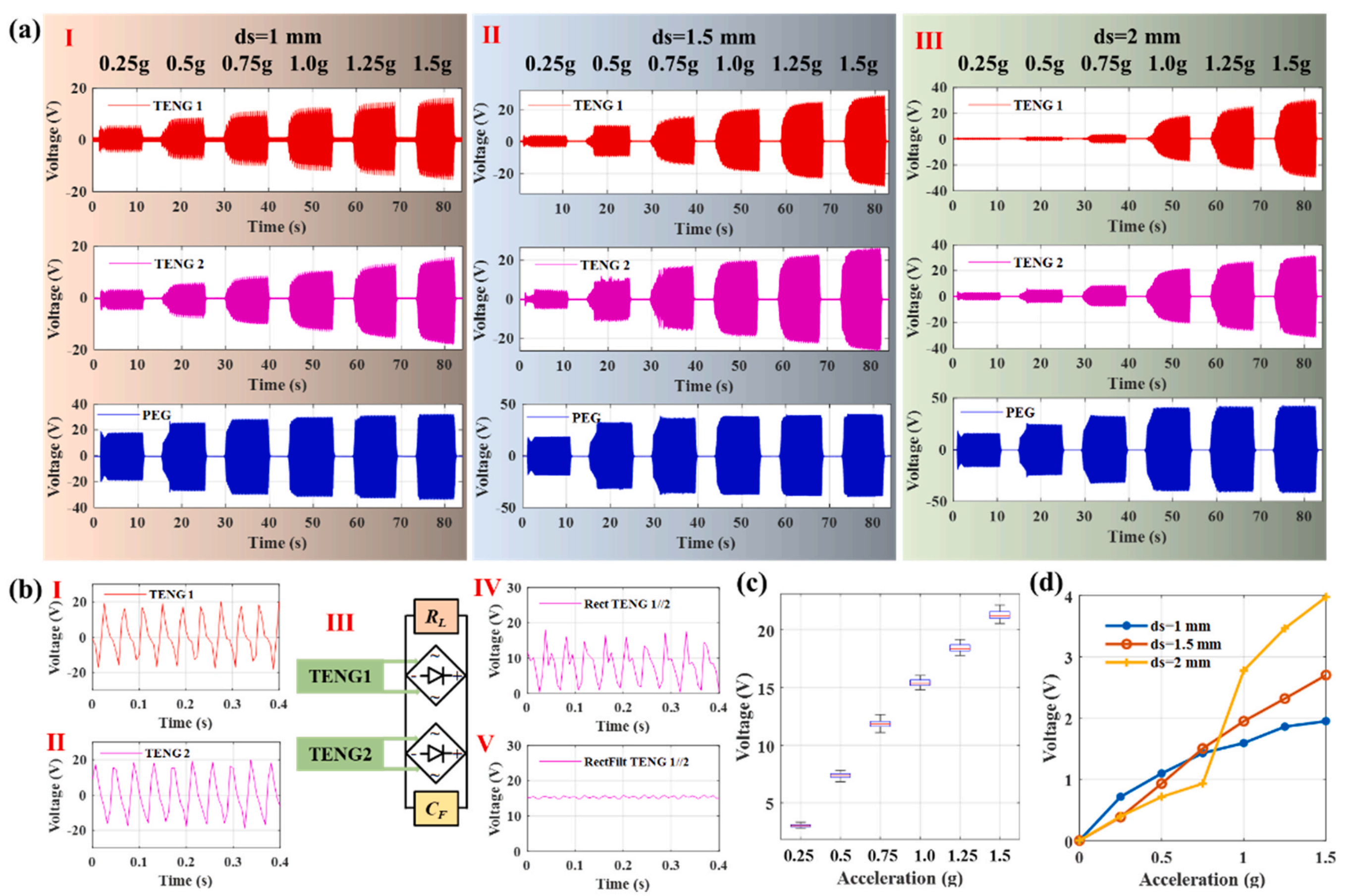

Fig. 3. (a) Experiment results: time response voltage curves of TENG1, TENG2, PEG with different ds = 1.0 1.5 2.0 mm under different accelerations at 25 Hz. (b) Rectified filter signal process of TENG by circuit (III): original signal of TENG1 (I) and TENG2 (II) are rectified separately before parallel connection (IV) and then filter as a stable signal (V). (c) Acceleration calibration curve of TENG accelerometer with ds = 1.5 mm. (d) Arduino analogy voltage curve of TENG accelerometer with different stopper distance.

desirable for both energy harvesting and acceleration sensing in the hybrid system. The discussion of the acceleration sensing mechanism and parameter optimization contribute to the design of the TENG accelerometer.

5. Application of PEG

PEG with broadband and adjustable resonant frequency can be used in energy harvesting at fixed frequency with small frequency drift or shock excitation. RMS voltage at the load resistance is get by a rectified filter interface circuit. RMS power is calculated by $P_{RMS} = V_{RMS}^2/R_L$. Fig. 4(a) shows RMS voltage and power response curves of TENG (TENG1 and TENG2 regulated before parallel connection) at different load resistances under a sine acceleration of 1 g at 25 Hz. Fig. 4(b) shows those of PEG. The maximum RMS power of TENG is 3.07 μW at optimal load resistance of 33 MΩ. The maximum RMS power of PEG is 6.5 mW at optimal load resistance of 40 kΩ. This is a pretty good output compared to the published performances of low frequency PZT piezoelectric energy harvesters (Table S2). Since the maximum RMS power of PEG is almost two thousand times that of TENG under the same excitation conditions, PEG is more suitable to be an energy harvester due to the mW level power output and TENG is preferable to be a self-powered accelerometer due to the good sensing linearity.

Fig. 4(c) shows PEG charge curves of different capacitors under 1 g acceleration at 25 Hz. It can charge a capacitor of 330 μF to 26 V quickly in 20 s. It is hopeful to supply power for many electronic devices. To increase the voltage amplitude, a double voltage rectifier circuit is designed in this work, as shown in Fig. 4(d). Compared to rectifier circuit, the negative end of the PEG and an alternating current (AC) terminal are short circuited in double voltage rectifier circuit. The AC voltage curve from − 30–30 V is then translated into a DC voltage curve from 0 V to 60 V, with an improvement of 100% compared to the conventional rectifier circuit with a DC voltage curve from 0 V to 30 V. After a double voltage rectifier circuit, the PEG can light up 30 LEDs in serial connections under 1 g acceleration at 25 Hz.

The bigger acceleration, the higher PEG output voltage, the more LEDs in serial connection can be light on. Base on that, the alarm acceleration level can be directly set as the number of LEDs in serial connection. When PEG is excited below the alarm acceleration level, no LEDs will be light up. When PEG is excited beyond the alarm acceleration level, LEDs will be light up flashing light to transmit the alarm signal.

Besides sine vibration detection, an SOS shaped 20 LEDs in serial connection is developed in shock-based vibration detection, as shown in Fig. 4(e). Attenuated oscillation waveform with peak voltage of 50 V is shown after a double voltage rectifier circuit. It can flash SOS LED sign in every shock excitation. This can be utilized in landslide, cargo, or human drop monitoring.

6. Self-sustained autonomous wireless sensing

Despite TENG has shown good linearity as a self-powered accelerometer and PEG has shown the milli-watt level power output, there are still some works to do to achieve a self-sustained autonomous wireless sensing system. It includes the low power consumption design and the power management circuit design. The IoT application topology is shown in Fig. 5(a–c). The autonomous WSN consists of a hybrid generator, an LTC-3588-1 based power management circuit, two energy storage capacitors, an Arduino nano development board as MCU, and a DL-20 CC2530 A as RF transceiver. The host computer consists of a DL-20 CC2530 B as an RF transceiver, a USB to TTL serial port as an interface converter, and a laptop to show the received wireless signal. The communication between autonomous WSN and host computer base on the Zigbee in IEEE 802.15.4 international standard. It is a low power communication with a physical wireless range of 10–20 m.

The autonomous WSN circuit design is depicted in Fig. 5(b). The PEG provides AC voltages to PZ1 and PZ1. It has a 2.7–20 V input operating range and will be rectified and filtered in V_{in} and stored in capacitor C_{in}

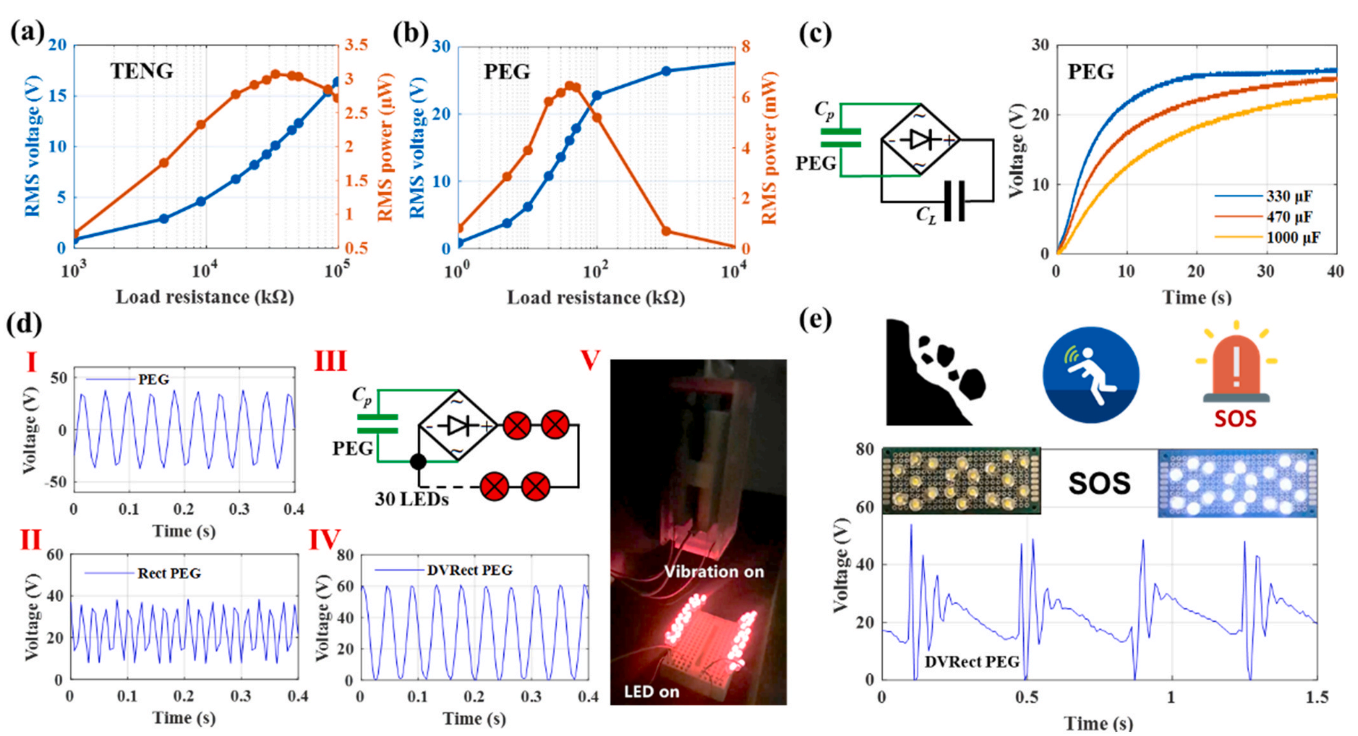

Fig. 4. RMS voltage and power response curves at different load resistance under 1 g acceleration at 25 Hz (a) PEG regulated, (b) TENG1 and TENG2 regulated before parallel connection. (c) PEG charge curves of different capacitors under 1 g acceleration at 25 Hz. (d) Double voltage rectifier circuit (III) for PEG to light up 30 LEDs (V) in serial connection under 1 g acceleration at 25 Hz; (I) original signal of PEG; (II) conventional rectified signal; (IV) double voltage rectified signal. (e) impulse signal of PEG to light up alarm LEDs.

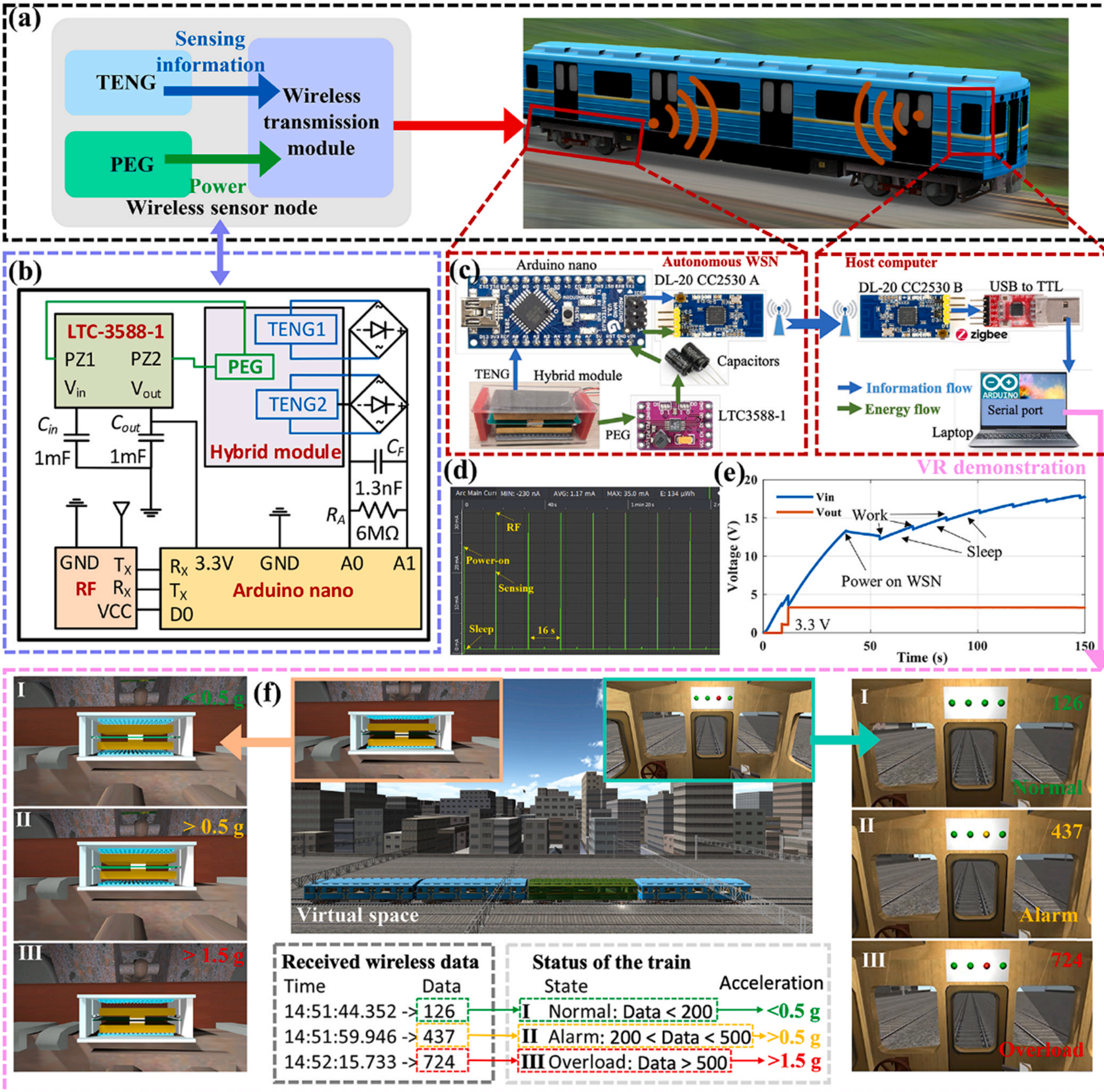

Fig. 5. Demonstration of self-sustained autonomous wireless sensing system: (a) Schematic showing the connection and function of the components in the wireless sensing system. (b) Autonomous WSN circuit design. (c) IoT application topology. (d) Current consumption curve of MCU and RF in low power consumption mode. (e) Voltage curves of capacitor charging in LTC3588-1; (f) VR demonstration of monitoring status of the train, and wireless acceleration data stream received in serial port software on the host computer.

of 1 mF. When 3.3 V output in V_{out} is selected, under-voltage lockout (UVLO) in the chip will work from 3.67 V to 5.05 V. Capacitor C_{out} of 1 mF is utilized to stable load voltage to power Arduino nano in case of instantaneous large discharge. TENG1 and TENG2 are rectified and parallel connected, and a filter capacitor C_F of 1.3nF and an adjust resistance R_A of 6 MΩ are parallel connected to give a stable and suitable voltage signal. The voltage difference in A0 and A1 is linearly proportional to the amplitude of acceleration. The code in Arduino nano (Note S3) will read the analog port voltage and convert it into a digital signal to be sent to the RF transceiver.

Low power consumption design is of crucial importance in a self-sustained system. The current consumption curve of MCU and RF in normal operation mode indicates an average current of 33 mA (MCU 3 mA and RF 30 mA) in 5 V power supply (Fig. S5). Such 165 mW power consumption is far beyond the transit output power capability of the PEG. Therefore, the hardware and the program are modified into low power consumption mode. The low dropout regulator (LDO) and power LED in Arduino nano are removed, the input voltage can be decreased from 5 V to 3.3 V and additional current consumption of 2 mA in Arduino nano will be avoided. The current consumption of RF transceiver accounts for a large proportion. Only intermittent power supply can reduce average power consumption. Therefore, a 16 s sleep mode is set in every duty by coding in Arduino nano. D0 is also set to high of 3.3 V to supply power for RF transceiver in 0.2 s work and set low to power off for RF transceiver in 16 s sleep. The current consumption curve of MCU and RF in low power consumption mode is shown in Fig. 5(d). Such a low duty cycle of 1.2% can ensure a low average current consumption of 1.17 mA in 3.3 V voltage supply.

Voltage curves of capacitor charging in LTC3588-1 by PEG in 1 g acceleration at 25 Hz for self-sustained autonomous wireless sensing are shown in Fig. 5(e). UVLO will allow V_{in} reaches 5 V before charge V_{out} into 3.3 V. V_{out} is stable at 3.3 V from 10 s and V_{in} reaches 13.5 V at 40 s, the power switch of WSN is turned on manually. Although the slow drop in V_{in} for startup power consumption and quickly drop in V_{in} for RF and TENG sensor work power consumption of 0.2 s, V_{in} will keep arising in a sleep period of 16 s. The overall upward trend of V_{in} shows that the self-power system is sustainable.

In future, we plan to apply this WSN for abnormal vibration monitoring of various equipment, such as drilling in mining, bridges, and train rails, whose working status can be continuously monitored by embedded accelerometers, revealing the irregular vibration incidents where an abnormal acceleration value is detected. To illustrate the feasibility of such applications, we created a virtual reality (VR) environment where a visual train is moving continuously with accelerometers embedded in each cabin for its status monitoring. A visualization panel with four LEDs corresponding to each cabin is built up in the operation room, which indicates the working status of the moving train intuitively based on the detected sensing signals from the accelerometer. Supplementary Video 4 shows the application of train monitoring with our self-sustainable WSN that functions as the self-powered accelerometer in cabin 3 in the VR environment.

Supplementary material related to this article can be found online at doi:10.1016/j.nanoen.2020.105555.

In the practical testing, we use the vibrational shaker to generate vibration source with a set-up frequency and acceleration to mimic the vibration of a moving train. The TENG acceleration sensing signal will be sent by RF transceiver and received on the host computer. The acceleration data stream received in serial port software is shown in Fig. 5(f). The bigger received data, the heavier vibration acceleration state. The acceleration data threshold can be set in the program to indicate the state of the vibration. Here, the received data is categorized into three ranges: below 200 ($<$ 0.5 g), between 200 and 500 ($>$ 0.5 g), and above 500 ($>$ 1.5 g), which correspond to three working status: normal, alarm, and overload.

The VR environment for train monitoring is presented in Fig. 5(f), in which the WSN is mounted on the axial box of the train to keep track of the vibration status of it. Correspondingly, there will be a display panel in the main control room indicating the detected status of the train. Here we have built a virtual train with four discrete cabins, and the WSN that is mounted on the testing shaker is set as the acceleration sensor in cabin 3 in the virtual space. The vibration status of the testing shaker stimulates the real vibration of the moving train, which can be intuitively observed from the light color of the display panel. To mimic the real applications, the vibration acceleration of the train will be increased by wear and crack of shafting, which would pose a great danger to the passengers if it is not timely noticed. Three different states of the WSN and display panel in this simulation test are shown in Fig. 5(f). As the train moves regularly, the acceleration level (in cabin 3) is measured below 0.5 g with the 3rd light showing the green light. When the axial box has an acceleration value larger than 0.5 g, the 3rd light will be turned yellow by the WSN, transmitting the alarm signal to the engineers in the main control room. Once the acceleration level is detected exceeding 1.5 g, the 3rd light will be converted into red immediately to warn the engineers about the detected overload situation in cabin 3. Extending the WSN numbers and monitoring areas, the whole train can be continuously monitored to ensure a safe trip along the journey. This VR demonstration has successfully indicated the great potential of the self-sustainable WSN for diversified machine/robot monitoring applications under the IoT framework in harsh environments and remote areas. Furthermore, various self-powered gas sensors could be integrated with our hybridized TENG and PEG vibration mechanism for toxic gas detection in harsh environments, e.g., coal mine, tunnel and chemical factory, etc [82,83].

7. Conclusions

This paper proposed a self-sustainable WSN consisting of a hybrid PEG and TENG vibration module. PEG not only shows broadband vibration behavior when it impacts with TENG, but also has the frequency tuning ability by applying an axial force. The PEG has a RMS power of 6.5 mW in 1.0 g acceleration at 25 Hz as an energy harvester. A double voltage rectifier circuit is proposed to double increase voltage output of PEG. It also shows good capability in light up 30 serial LEDs in sine vibration and 20 serial LEDs in shock vibration, which can function as alarming signals in vibration and drop monitoring. Good linearity with a sensitivity of 15 V/g (0–1.5 g) has been achieved with the self-powered triboelectric accelerometer, which has an optimized separation gap of 1.5 mm. Finally, a self-sustained autonomous WSN is achieved based on a hybridized TENG and PEG vibration mechanism, with the PEG serving as the energy source and the TENG functions as the self-powered sensing unit. The feasibility of train status monitoring of the self-sustainable WSN has been demonstrated with the VR train monitoring test. Looking forward, the self-sustainable WSN as a great prospect in the eventual realization of self-sustainable monitoring systems in remote areas and harsh environments.

8. Methods

8.1. Preparation hybrid TENG and PEG vibration module

PMMA package is fabricated by laser cutting. Two hinged supporters are fabricated by 3D printing to hold two sides of the PZT bimorph (http://www.pantpiezo.com). Eco flex with pyramidal synaptic array structure is made from the 3D printing mold (Fig. S6). Geometry parameters of hybrid TENG and PEG vibration modules can be found in Table S3.

8.2. Vibration and power consumption test

The vibration test platform is shown in (Fig. S7). PC software sets test parameters, including sweep frequency range and vibration amplitude. Vibration controller signals are amplified by power amplifier type 2718 and then fed to the exciter WA-0308. The feedback signal is measured by an acceleration sensor CXL10GP3. The load resistance of PEG is adjusted by the resistance decade model 610. Vibration controller type 7541 also harvests voltage signals in the time domain, which are transformed into frequency domain signals through FFT changes of PC software.

The open-circuit voltage and capacitors charging curves were measured by an oscilloscope (Agilent, InfiniVision, DSO-X 3034A) and a high voltage probe (Keysight N2771B). The current consumption of WSN was tested by a power source (Otii LPA375).

Data availability

The data that support the findings of this study are available from the corresponding authors upon reasonable request.

CRediT authorship contribution statement

Lu Wang: Data curation, Writing - original draft. **Tianyiyi He:** Revise manuscript. **Zixuan Zhang:** Software. **Libo Zhao:** Conceptualization, Methodology. **Chengkuo Lee:** Writing - review & editing. **Guoxi Luo, Qi Mao:** Visualization, Investigation. **Ping Yang, Qijing Lin:** Funding acquisition. **Xiang Li, Ryutaro Maeda:** Supervision. **Zhuangde Jiang:** Project administration.

Declaration of Competing Interest

The authors declare that they have no known competing financial interests or personal relationships that could have appeared to influence the work reported in this paper.

Acknowledgements

This work was supported in part by the National Key Research & Development (R&D) Program of China, China (Grant No. 2016YFB1200100), the National Natural Science Foundation of China, China (Grant Nos. 91748207, 51875449, 51705409), and the 111 Program, China (Grant No. B12016). Besides, this work is aprtly supported by National Key Research and Development (R&D) Program of China, China (Grant No. 2019YFB2004800, Project No. R-2020-S-002) at the NUSRI, Suzhou, China, and the RIE 2020-AME-2019-Nanosystems at the Edge grant, Singapore (R-263-000-D67-305) at the NUS, Singapore.

Appendix A. Supporting information

Supplementary data associated with this article can be found in the online version at doi:10.1016/j.nanoen.2020.105555.

References

[1] X. Liang, T. Jiang, G. Liu, Y. Feng, C. Zhang, Z.L. Wang, Spherical triboelectric nanogenerator integrated with power management module for harvesting multidirectional water wave energy, Energy Environ. Sci. 13 (1) (2020) 277–285, https://doi.org/10.1039/c9ee03258d.

[2] W. Tang, C.B. Han, C. Zhang, Z.L. Wang, Cover-sheet-based nanogenerator for charging mobile electronics using low-frequency body motion/vibration, Nano Energy 9 (2014) 121–127, https://doi.org/10.1016/j.nanoen.2014.07.005.

[3] Y. Zi, J. Wang, S. Wang, S. Li, Z. Wen, H. Guo, Z.L. Wang, Effective energy storage from a triboelectric nanogenerator, Nat. Commun. 7 (2016) 10987, https://doi.org/10.1038/ncomms10987.

[4] Y.-T. Jao, P.K. Yang, C.M. Chiu, Y.J. Lin, S.W. Chen, D. Choi, Z.H. Lin, A textile-based triboelectric nanogenerator with humidity-resistant output characteristic and its applications in self-powered healthcare sensors, Nano Energy 50 (2018) 513–520, https://doi.org/10.1016/j.nanoen.2018.05.071.

[5] N. Li, Z. Yi, Y. Ma, F. Xie, Y. Huang, Y. Tian, X. Dong, Y. Liu, X. Shao, Y. Li, L. Jin, J. Liu, Z. Xu, B. Yang, H. Zhang, Direct powering a real cardiac pacemaker by natural energy of a heartbeat, ACS Nano 13 (3) (2019) 2822–2830, https://doi.org/10.1021/acsnano.8b08567.

[6] H. Yang, M. Wang, M. Deng, H. Guo, W. Zhang, H. Yang, Y. Xi, X. Li, C. Hu, Z. Wang, A full-packaged rolling triboelectric-electromagnetic hybrid nanogenerator for energy harvesting and building up self-powered wireless systems, Nano Energy 56 (2019) 300–306, https://doi.org/10.1016/j.nanoen.2018.11.043.

[7] H. Ryu, H.J. Yoon, S.W. Kim, Hybrid energy harvesters: toward sustainable energy harvesting, Adv. Mater. 31 (34) (2019), e1802898, https://doi.org/10.1002/adma.201802898.

[8] C. Bao Han, C. Zhang, X.H. Li, L. Zhang, T. Zhou, W. Hu, Z. Lin Wang, Self-powered velocity and trajectory tracking sensor array made of planar triboelectric nanogenerator pixels, Nano Energy 9 (2014) 325–333, https://doi.org/10.1016/j.nanoen.2014.07.025.

[9] T. Bu, L. Xu, Z. Yang, X. Yang, G. Liu, Y. Cao, C. Zhang, Z.L. Wang, Nanoscale triboelectrification gated transistor, Nat. Commun. 11 (1) (2020) 1054, https://doi.org/10.1038/s41467-020-14909-6.

[10] Aminullah, A.K. Kasi, J.K. Kasi, M. Uddin, M. Bokhari, Triboelectric nanogenerator as self-powered impact force sensor for falling object, Curr. Appl. Phys. 20 (1) (2020) 137–144, https://doi.org/10.1016/j.cap.2019.10.016.

[11] X. Zhao, Z. Kang, Q. Liao, Z. Zhang, M. Ma, Q. Zhang, Y. Zhang, Ultralight, self-powered and self-adaptive motion sensor based on triboelectric nanogenerator for perceptual layer application in Internet of things, Nano Energy 48 (2018) 312–319, https://doi.org/10.1016/j.nanoen.2018.03.072.

[12] Q. Zhang, Q. Liang, Q. Liao, F. Yi, X. Zheng, M. Ma, F. Gao, Y. Zhang, Service behavior of multifunctional triboelectric nanogenerators, Adv. Mater. 29 (17) (2017) 1606703, https://doi.org/10.1002/adma.201606703.

[13] X. Pu, H. Guo, Q. Tang, J. Chen, L. Feng, G. Liu, X. Wang, Y. Xi, C. Hu, Z.L. Wang, Rotation sensing and gesture control of a robot joint via triboelectric quantization sensor, Nano Energy 54 (2018) 453–460, https://doi.org/10.1016/j.nanoen.2018.10.044.

[14] T. Chen, Q. Shi, M. Zhu, T. He, Z. Yang, H. Liu, L. Sun, L. Yang, C. Lee, Intuitive-augmented human-machine multidimensional nano-manipulation terminal using triboelectric stretchable strip sensors based on minimalist design, Nano Energy 60 (2019) 440–448, https://doi.org/10.1016/j.nanoen.2019.03.071.

[15] Q. Liang, Z. Zhanga, X. Yan, Y. Gu, Y. Zhao, G. Zhang, S. Lu, Q. Liao, Y. Zhang, Functional triboelectric generator as self-powered vibration sensor with contact mode and non-contact mode, Nano Energy 14 (2015) 209–216, https://doi.org/10.1016/j.nanoen.2014.07.010.

[16] J. Chen, H. Guo, Z. Wu, G. Xu, Y. Zi, C. Hu, Z.L. Wang, Actuation and sensor integrated self-powered cantilever system based on TENG technology, Nano Energy 64 (2019), 103920, https://doi.org/10.1016/j.nanoen.2019.103920.

[17] F. Xi, Y. Pang, G. Liu, S. Wang, W. Li, C. Zhang, Z.L. Wang, Self-powered intelligent buoy system by water wave energy for sustainable and autonomous wireless sensing and data transmission, Nano Energy 61 (2019) 1–9, https://doi.org/10.1016/j.nanoen.2019.04.026.

[18] D. Liu, B. Chen, J. An, C. Li, G. Liu, J. Shao, W. Tang, C. Zhang, Z.L. Wang, Wind-driven self-powered wireless environmental sensors for Internet of Things at long distance, Nano Energy 73 (2020), 104819, https://doi.org/10.1016/j.nanoen.2020.104819.

[19] H.-J. Yoon, S.-W. Kim, Nanogenerators to power implantable medical systems, Joule 4 (7) (2020) 1398–1407, https://doi.org/10.1016/j.joule.2020.05.003.

[20] X. Fan, J. He, J. Mu, J. Qian, N. Zhang, C. Yang, X. Hou, W. Geng, X. Wang, X. Chou, Triboelectric-electromagnetic hybrid nanogenerator driven by wind for self-powered wireless transmission in Internet of Things and self-powered wind speed sensor, Nano Energy 68 (2019), 104319, https://doi.org/10.1016/j.nanoen.2019.104319.

[21] S. Mekid, A. Bouhraoua, U. Baroudi, Battery-less wireless remote bolt tension monitoring system, Mech. Syst. Signal Process. 128 (2019) 572–587, https://doi.org/10.1016/j.ymssp.2019.04.022.

[22] Z. Xie, Z. Zeng, Y. Wang, W. Yang, Y. Xu, X. Lu, T. Cheng, H. Zhao, Z.L. Wang, Novel sweep-type triboelectric nanogenerator utilizing single freewheel for random triggering motion energy harvesting and driver habits monitoring, Nano Energy 68 (2020), 104360, https://doi.org/10.1016/j.nanoen.2019.104360.

[23] H. Askari, A. Khajepour, M.B. Khamesee, Z.L. Wang, Embedded self-powered sensing systems for smart vehicles and intelligent transportation, Nano Energy 66 (2019), 104103, https://doi.org/10.1016/j.nanoen.2019.104103.

[24] L. Jin, W. Deng, Y. Su, Z. Xu, H. Meng, B. Wang, H. Zhang, B. Zhang, L. Zhang, X. Xiao, M. Zhu, W. Yang, Self-powered wireless smart sensor based on maglev porous nanogenerator for train monitoring system, Nano Energy 38 (2017) 185–192, https://doi.org/10.1016/j.nanoen.2017.05.018.

[25] M. Gao, J. Cong, J. Xiao, Q. He, S. Li, Y. Wang, Y. Yao, R. Chen, P. Wang, Dynamic modeling and experimental investigation of self-powered sensor nodes for freight rail transport, Appl. Energy 257 (2020), 113969, https://doi.org/10.1016/j.apenergy.2019.113969.

[26] M. Khazaee, A. Rezaniakolaie, A. Moosavian, L. Rosendahl, A novel method for autonomous remote condition monitoring of rotating machines using piezoelectric energy harvesting approach, Sens. Actuators A Phys. 295 (2019) 37–50, https://doi.org/10.1016/j.sna.2019.05.016.

[27] L. Lu, Y. He, T. Wang, T. Shi, B. Li, Self-powered wireless sensor for fault diagnosis of wind turbine planetary gearbox, IEEE Access 7 (2019) 87382–87395, https://doi.org/10.1109/access.2019.2925426.

[28] Z. Wang, Y. Cheng, P. Allen, Z. Yin, D. Zou, W. Zhang, Analysis of vibration and temperature on the axle box bearing of a high-speed train, Veh. Syst. Dyn. 58 (2019) 1–24, https://doi.org/10.1080/00423114.2019.1645340.

[29] B. Zhang, A.C.C. Tan, J.-h Lin, Gearbox fault diagnosis of high-speed railway train, Eng. Fail. Anal. 66 (2016) 407–420, https://doi.org/10.1016/j.engfailanal.2016.04.020.

[30] X. Zhao, G. Wei, X. Li, Y. Qin, D. Xu, W. Tang, H. Yin, X. Wei, L. Jia, Self-powered triboelectric nano vibration accelerometer based wireless sensor system for railway state health monitoring, Nano Energy 34 (2017) 549–555, https://doi.org/10.1016/j.nanoen.2017.02.036.

[31] K.H. Koh, Q. Shi, S. Cao, D. Ma, H.Y. Tan, Z. Guo, C. Lee, A self-powered 3D activity inertial sensor using hybrid sensing mechanisms, Nano Energy 56 (2019) 651–661, https://doi.org/10.1016/j.nanoen.2018.11.075.

[32] Z. Wu, W. Ding, Y. Dai, K. Dong, C. Wu, L. Zhang, Z. Lin, J. Cheng, Z.L. Wang, Self-powered multifunctional motion sensor enabled by magnetic-regulated triboelectric nanogenerator, ACS Nano 12 (6) (2018) 5726–5733, https://doi.org/10.1021/acsnano.8b01589.

[33] Q. Shi, H. Wu, H. Wang, H. Wu, C. Lee, Self-powered gyroscope ball using a triboelectric mechanism, Adv. Energy Mater. 7 (22) (2017) 1701300, https://doi.org/10.1002/aenm.201701300.

[34] H. Yu, X. He, W. Ding, Y. Hu, D. Yang, S. Lu, C. Wu, H. Zou, R. Liu, C. Lu, Z. L. Wang, A self-powered dynamic displacement monitoring system based on triboelectric accelerometer, Adv. Energy Mater. 7 (19) (2017) 1700565, https://doi.org/10.1002/aenm.201700565.

[35] R.K. Gupta, Q. Shi, L. Dhakar, T. Wang, C.H. Heng, C. Lee, Broadband energy harvester using non-linear polymer spring and electromagnetic/triboelectric hybrid mechanism, Sci. Rep. 7 (2017) 41396, https://doi.org/10.1038/srep41396.

[36] C. Liu, Y. Wang, N. Zhang, X. Yang, Z. Wang, L. Zhao, W. Yang, L. Dong, L. Che, G. Wang, X. Zhou, A self-powered and high sensitivity acceleration sensor with V-Q-a model based on triboelectric nanogenerators (TENGs), Nano Energy 67 (2020), 104228, https://doi.org/10.1016/j.nanoen.2019.104228.

[37] Q. Zhang, Q. Liang, D.K. Nandakumar, S.K. Ravi, H. Qu, L. Suresh, X. Zhang, Y. Zhang, L. Yang, A. Wee, S.C. Tan, Energy harvesting from shadow-effect, Energy Environ. Sci. 13 (2020) 2404–2413, https://doi.org/10.1039/d0ee00825g.

[38] Q. Zeng, Y. Wu, Q. Tang, W. Liu, J. Wu, Y. Zhang, G. Yin, H. Yang, S. Yuan, D. Tan, C. Hu, X. Wang, A high-efficient breeze energy harvester utilizing a full-packaged triboelectric nanogenerator based on flow-induced vibration, Nano Energy 70 (2020), 104524, https://doi.org/10.1016/j.nanoen.2020.104524.

[39] H. Liu, J. Zhong, C. Lee, S.-W. Lee, L. Lin, A comprehensive review on piezoelectric energy harvesting technology: materials, mechanisms, and applications, Appl. Phys. Rev. 5 (4) (2018), 041306, https://doi.org/10.1063/1.5074184.

[40] L. Zheng, Z.H. Lin, G. Cheng, W. Wu, X. Wen, S. Lee, Z.L. Wang, Silicon-based hybrid cell for harvesting solar energy and raindrop electrostatic energy, Nano Energy 9 (2014) 291–300, https://doi.org/10.1016/j.nanoen.2014.07.024.

[41] C. Hou, T. Chen, Y. Li, M. Huang, Q. Shi, H. Liu, L. Sun, C. Lee, A rotational pendulum based electromagnetic/triboelectric hybrid-generator for ultra-low-frequency vibrations aiming at human motion and blue energy applications, Nano Energy 63 (2019), 103871, https://doi.org/10.1016/j.nanoen.2019.103871.

[42] J. Luo, Z.L. Wang, Recent advances in triboelectric nanogenerator based self-charging power systems, Energy Storage Mater. 23 (2019) 617–628, https://doi.org/10.1016/j.ensm.2019.03.009.

[43] C. Sun, Q. Shi, D. Hasan, M.S. Yazici, M. Zhu, Y. Ma, B. Dong, Y. Liu, C. Lee, Self-powered multifunctional monitoring system using hybrid integrated triboelectric nanogenerators and piezoelectric microsensors, Nano Energy 58 (2019) 612–623, https://doi.org/10.1016/j.nanoen.2019.01.096.

[44] L. Gao, S. Lu, W. Xie, X. Chen, L. Wu, T. Wang, A. Wang, C. Yue, D. Tong, W. Lei, H. Yu, X. He, X. Mu, Z.L. Wang, Y. Yang, A self-powered and self-functional tracking system based on triboelectric-electromagnetic hybridized blue energy harvesting module, Nano Energy 72 (2020), 104684, https://doi.org/10.1016/j.nanoen.2020.104684.

[45] X. Zhong, Y. Yang, X. Wang, Z.L. Wang, Rotating-disk-based hybridized electromagnetic-triboelectric nanogenerator for scavenging biomechanical energy as a mobile power source, Nano Energy 13 (2015) 771–780, https://doi.org/10.1016/j.nanoen.2015.03.012.

[46] J. Zhao, G. Zhen, G. Liu, T. Bu, W. Liu, X. Fu, P. Zhang, C. Zhang, Z.L. Wang, Remarkable merits of triboelectric nanogenerator than electromagnetic generator for harvesting small-amplitude mechanical energy, Nano Energy 61 (2019) 111–118, https://doi.org/10.1016/j.nanoen.2019.04.047.

[47] X. Xiao, X. Zhang, S. Wang, H. Ouyang, P. Chen, L. Song, H. Yuan, Y. Ji, P. Wang, Z. Li, M. Xu, Z.L. Wang, Honeycomb structure inspired triboelectric nanogenerator for highly effective vibration energy harvesting and self-powered engine condition monitoring, Adv. Energy Mater. 9 (40) (2019) 1902460, https://doi.org/10.1002/aenm.201902460.

[48] J. He, T. Wen, S. Qian, Z. Zhang, Z. Tian, J. Zhu, J. Mu, X. Hou, W. Geng, J. Cho, J. Han, X. Chou, C. Xue, Triboelectric-piezoelectric-electromagnetic hybrid nanogenerator for high-efficient vibration energy harvesting and self-powered wireless monitoring system, Nano Energy 43 (2018) 326–339, https://doi.org/10.1016/j.nanoen.2017.11.039.

[49] L. Wang, J. Ding, Z. Jiang, G. Luo, L. Zhao, D. Lu, X. Yang, M. Ryutaro, A packaged piezoelectric vibration energy harvester with high power and broadband characteristics, Sens. Actuators A Phys. 295 (2019) 629–636, https://doi.org/10.1016/j.sna.2019.06.034.

[50] Y. Tian, G. Li, Z. Yi, J. Liu, B. Yang, A low-frequency MEMS piezoelectric energy harvester with a rectangular hole based on bulk PZT film, J. Phys. Chem. Solids 117 (2018) 21–27, https://doi.org/10.1016/j.jpcs.2018.02.024.

[51] K. Zhou, H.L. Dai, A. Abdelkefi, Q. Ni, Theoretical modeling and nonlinear analysis of piezoelectric energy harvesters with different stoppers, Int. J. Mech. Sci. 166 (2020), 105233, https://doi.org/10.1016/j.ijmecsci.2019.105233.

[52] L. Wang, G. Luo, Z. Jiang, F. Zhang, L. Zhao, P. Yang, Q. Lin, R. Maeda, Broadband vibration energy harvesting for wireless sensor node power supply in train container, Rev. Sci. Instrum. 90 (12) (2019), 125003, https://doi.org/10.1063/1.5127243.

[53] H. Liu, C. Lee, T. Kobayashi, C.J. Tay, C. Quan, Investigation of a MEMS piezoelectric energy harvester system with a frequency-widened-bandwidth mechanism introduced by mechanical stoppers, Smart Mater. Struct. 21 (3) (2012), 035005, https://doi.org/10.1088/0964-1726/21/3/035005.

[54] H. Liu, C. Lee, T. Kobayashi, C.J. Tay, C. Quan, Piezoelectric MEMS-based wideband energy harvesting systems using a frequency-up-conversion cantilever stopper, Sens. Actuators A Phys. 186 (2012) 242–248, https://doi.org/10.1016/j.sna.2012.01.033.

[55] E.S. Leland, P.K. Wright, Resonance tuning of piezoelectric vibration energy scavenging generators using compressive axial preload, Smart Mater. Struct. 15 (5) (2006) 1413–1420, https://doi.org/10.1088/0964-1726/15/5/030.

[56] M.O. Mansour, M.H. Arafa, S.M. Megahed, Resonator with magnetically adjustable natural frequency for vibration energy harvesting, Sens. Actuators A Phys. 163 (1) (2010) 297–303, https://doi.org/10.1016/j.sna.2010.07.001.

[57] W. Kim, D. Bhatia, S. Jeong, D. Choi, Mechanical energy conversion systems for triboelectric nanogenerators: Kinematic and vibrational designs, Nano Energy 56 (2019) 307–321, https://doi.org/10.1016/j.nanoen.2018.11.056.

[58] F. Ali, W. Raza, X. Li, H. Gul, K.-H. Kim, Piezoelectric energy harvesters for biomedical applications, Nano Energy 57 (2019) 879–902, https://doi.org/10.1016/j.nanoen.2019.01.012.

[59] H. Deng, J. Ye, Y. Du, J. Zhang, M. Ma, X. Zhong, Bistable broadband hybrid generator for ultralow-frequency rectilinear motion, Nano Energy 65 (2019), 103973, https://doi.org/10.1016/j.nanoen.2019.103973.

[60] X. He, Q. Wen, Y. Sun, Z. Wen, A low-frequency piezoelectric-electromagnetic-triboelectric hybrid broadband vibration energy harvester, Nano Energy 40 (2017) 300–307, https://doi.org/10.1016/j.nanoen.2017.08.024.

[61] C. Liu, N. Zhang, J. Li, et al., Harvesting ultralow frequency (< 1 Hz) mechanical energy using triboelectric nanogenerator, Nano Energy 65 (2019), https://doi.org/10.1016/j.nanoen.2019.104011.

[62] W. Yang, J. Chen, G. Zhu, et al., Harvesting Energy from the Natural Vibration of Human Walking, Acs Nano 7 (12) (2013) 11317–11324.

[63] L. Dhakar, F.E.H. Tay, C. Lee, Investigation of contact electrification based broadband energy harvesting mechanism using elastic PDMS microstructures, J. Micromech. Microeng. 24 (10) (2014), 104002, https://doi.org/10.1088/0960-1317/24/10/104002.

[64] Z. Wen, H. Guo, Y. Zi, M.H. Yeh, X. Wang, J. Deng, J. Wang, S. Li, C. Hu, L. Zhu, Z. L. Wang, Harvesting broad frequency band blue energy by a triboelectric-electromagnetic hybrid nanogenerator", ACS Nano 10 (7) (2016) 6526–6534, https://doi.org/10.1021/acsnano.6b03293.

[65] D. Bhatia, W. Kim, S. Lee, S.W. Kim, D. Choi, Tandem triboelectric nanogenerators for optimally scavenging mechanical energy with broadband vibration frequencies, Nano Energy 33 (2017) 515–521, https://doi.org/10.1016/j.nanoen.2017.01.059.

[66] Q. Shi, H. Wang, H. Wu, C. Lee, Self-powered triboelectric nanogenerator buoy ball for applications ranging from environment monitoring to water wave energy farm, Nano Energy 40 (2017) 203–213, https://doi.org/10.1016/j.nanoen.2017.08.018.

[67] M. Han, X. Zhang, W. Liu, X. Sun, X. Peng, H. Zhang, Low-frequency wide-band hybrid energy harvester based on piezoelectric and triboelectric mechanism, Sci. China Technol. Sci. 56 (8) (2013) 1835–1841, https://doi.org/10.1007/s11431-013-5270-x.

[68] C. Zhao, Q. Zhang, W. Zhang, X. Du, Y. Zhang, S. Gong, K. Ren, Q. Sun, Z.L. Wang, Hybrid piezo/triboelectric nanogenerator for highly efficient and stable rotation energy harvesting, Nano Energy 57 (2019) 440–449, https://doi.org/10.1016/j.nanoen.2018.12.062.

[69] Z. Li, Z. Saadatnia, Z. Yang, H. Naguib, A hybrid piezoelectric-triboelectric generator for low-frequency and broad-bandwidth energy harvesting, Energy Convers. Manag. 174 (2018) 188–197, https://doi.org/10.1016/j.enconman.2018.08.018.

[70] L. Bu, Z. Chen, Z. Chen, L. Qin, F. Yang, K. Xu, J. Han, X. Wang, Impact induced compound method for triboelectric-piezoelectric hybrid nanogenerators to achieve Watt level average power in low frequency rotations, Nano Energy 70 (2020), 104500, https://doi.org/10.1016/j.nanoen.2020.104500.

[71] D. Jiang, H. Ouyang, B. Shi, Y. Zou, P. Tan, X. Qu, S. Chao, Y. Xi, C. Zhao, Y. Fan, Z. Li, A wearable noncontact free-rotating hybrid nanogenerator for self-powered electronics, InfoMat 2 (2020) 1191–1200, https://doi.org/10.1002/inf2.12103.

[72] B. Shi, Q. Zheng, W. Jiang, L. Yan, X. Wang, H. Liu, Y. Yao, Z. Li, Z.L. Wang, A packaged self-powered system with universal connectors based on hybridized nanogenerators, Adv. Mater. 28 (5) (2016) 846–852, https://doi.org/10.1002/adma.201503356.

[73] M. Zhu, Q. Shi, T. He, Z. Yi, Y. Ma, B. Yang, T. Chen, C. Lee, Self-powered and self-functional cotton sock using piezoelectric and triboelectric hybrid mechanism for healthcare and sports monitoring, ACS Nano 13 (2) (2019) 1940–1952, https://doi.org/10.1021/acsnano.8b08329.

[74] Y. Zou, J. Liao, H. Ouyang, D. Jiang, C. Zhao, Z. Li, X. Qu, Z. Liu, Y. Fan, B. Shi, L. Zheng, Z. Li, A flexible self-arched biosensor based on combination of piezoelectric and triboelectric effects, Appl. Mater. Today 20 (2020), 100699, https://doi.org/10.1016/j.apmt.2020.100699.

[75] J. Wan, H. Wang, L. Miao, X. Chen, Y. Song, H. Guo, C. Xu, Z. Ren, H. Zhang, A flexible hybridized electromagnetic-triboelectric nanogenerator and its application for 3D trajectory sensing, Nano Energy 74 (2020), 104878, https://doi.org/10.1016/j.nanoen.2020.104878.

[76] F. Wen, H. Wang, T. He, Q. Shi, Z. Sun, M. Zhu, Z. Zhang, Z. Cao, Y. Dai, T. Zhang, C. Lee, Battery-free short-range self-powered wireless sensor network (SS-WSN) using TENG based direct sensory transmission (TDST) mechanism, Nano Energy 67 (2019), 104266, https://doi.org/10.1016/j.nanoen.2019.104266.

[77] T. He, H. Wang, J. Wang, X. Tian, F. Wen, Q. Shi, J.S. Ho, C. Lee, Self-sustainable wearable textile nano-energy nano-system (NENS) for next-generation healthcare applications, Adv. Sci. (Weinh.) 6 (24) (2019) 1901437, https://doi.org/10.1002/advs.201901437.

[78] L. Liu, Q. Shi, C. Lee, A novel hybridized blue energy harvester aiming at all-weather IoT applications, Nano Energy 76 (2020), 105052, https://doi.org/10.1016/j.nanoen.2020.105052.

[79] A.A. Khan, A. Mahmud, S. Zhang, S. Islam, P. Voss, D. Ban, A self-powered multi-broadcasting wireless sensing system realized with an all-in-one triboelectric nanogenerator, Nano Energy 62 (2019) 691–699, https://doi.org/10.1016/j.nanoen.2019.05.073.

[80] S. Lu, L. Gao, X. Chen, D. Tong, W. Lei, P. Yuan, X. Mu, H. Yu, Simultaneous energy harvesting and signal sensing from a single triboelectric nanogenerator for intelligent self-powered wireless sensing systems, Nano Energy 75 (2020), 104813, https://doi.org/10.1016/j.nanoen.2020.104813.

[81] X. Chen, L. Gao, J. Chen, S. Lu, H. Zhou, T. Wang, A. Wang, Z. Zhang, S. Guo, X. Mu, Z.L. Wang, Y. Yang, A chaotic pendulum triboelectric-electromagnetic hybridized nanogenerator for wave energy scavenging and self-powered wireless sensing system, Nano Energy 69 (2020), 104440, https://doi.org/10.1016/j.nanoen.2019.104440.

[82] H. Wang, H. Wu, D. Hasan, T. He, Q. Shi, C. Lee, Self-powered dual-mode amenity sensor based on the water-air triboelectric nanogenerator, ACS Nano 11 (10) (2017) 10337–10346, https://doi.org/10.1021/acsnano.7b05213.

[83] F. Wen, T. He, H. Liu, H.-Y. Chen, T. Zhang, C. Lee, Advances in chemical sensing technology for enabling the next-generation self-sustainable integrated wearable system in the IoT era, Nano Energy 78 (2020), 105155, https://doi.org/10.1016/j.nanoen.2020.105155.

Lu Wang received the B.S. degree in Mechanical Engineering and Automation from Xi'an Jiaotong University in July 2013. Now he is pursuing the Ph.D. in Xi'an Jiaotong University, and one year exchange as visiting Ph.D in National University of Singapore. His research interests include energy harvesting, MEMS sensors and actuator, and structural vibration.

Tianyiyi He Received her B.Eng. degree from the School of Microelectronics and Solid-state Electronics at the University of Electronic Science and Technology of China (UESTC), Chengdu, China, in 2016, and will receive the Ph.D. degree from Department of Electrical and Computer Engineering at the National University of Singapore in 2020. She is currently a Research Fellow in the Dept. of ECE, NUS. Her research interests are focused on wearable energy harvesters and self-powered sensors.

Zixuan Zhang received his B.Eng. degree from the School of Mechanical and Electrical Engineering at the University of Electronic Science and Technology of China (UESTC), Chengdu, China, in 2018. After that he received his M.Sc. degree from Department of Electrical and Computer Engineering at National University of Singapore in 2019. Currently, he is a Research Assistant in the Dept. of ECE, NUS. His research interests are focused on energy harvesters, self-powered sensors and triboelectric nanogenerator.

Libo Zhao was born in Yantai, China, in 1978. He received M. S. degree in Instrument Science and Technology in 2003 and Ph.D. degree in Instrument Science and Technology in 2007, both from Xi'an Jiaotong University, Xi'an, China. He is currently working as an associate professor in Xi'an Jiaotong University. His research interests include micro and nano-fabrication technology, MEMS sensor technology and precision machining technology.

Chengkuo Lee received his Ph.D. degree in Precision Engineering from The University of Tokyo in 1996. Currently, he is the director of Center for Intelligent Sensors and MEMS at National University of Singapore, Singapore. In 2001, he cofounded Asia Pacific Microsystems, Inc., where he was the Vice President. From 2006–2009, he was a Senior Member of the Technical Staff at the Institute of Microelectronics, A-STAR, Singapore. He has contributed to more than 330 peer-reviewed international journal articles.

Guoxi Luo received the Ph.D. degree in Instrument Science and Technology in 2016 from Chongqing University, Chongqing, China. He is currently working as an assistant professor in Xi'an Jiaotong University. His research interests include micro and nanofabrication technology, nano energy harvesting technology, and electrochemistry.

Ryutaro Maeda has joined to Mechanical Engineering Laboratory, Agency of Advanced Industrial Science and Technology (AIST) in Tsukuba in 1980, after finishing Master course in Graduate School of Tokyo University. He is founder of UMEMSME (Research Centre of Ubiquitous MEMS and Micro Engineering) in AIST, and has been Director from 2010 to 2014 and served as Leader of several National Projects, including Ā Green Sensor Networkā , JST CREST program, etc. He is also a Professor at Xi'an Jiaotong University since 2018. His current research interest includes application of wireless networked sensing for energy and safety management, and published more than 300 papers in MEMS and related fields.

Zhuangde Jiang, Ph.D., professor of Xi'an Jiaotong University, academician of Chinese Academy of Engineering. He is currently the director of Institute of Precision Engineering (IPE). He is also the vice director of Chinese Society of Micro-Nano Technology (CSMNT) and the executive director of Chinese Mechanical Engineering Society (CMES). He involves in research areas including Micro-Nano fabrication technology, Micro Electro-Mechanical System (MEMS) and sensor technology, ultra-precision machining technology and equipment, photoelectric testing technology and instrumentation, etc.